Received: 5 August 2022 | Revised: 27 October 2022 | Accepted: 15 November 2022

IET Renewable Power Generation

DOI: 10.1049/rpg2.12646

The Institution of Engineering and Technology WILEY

ORIGINAL RESEARCH

A study on the effects of electromagnetic coupling mechanisms in the event of an indirect lightning strike near photovoltaic arrays

Jesús De La Casa Hernández[1] | **Francisco José Sánchez Sutil**[1] | **Carlo Petrarca**[2] | **Alessandro Formisano**[3]

[1]Department of Electrical Engineering, Universidad de Jaen, Campus Lagunillas s/n, Edificio A3, Jaén, Spain

[2]Department of Electric Engineering and Information Technology, Università di Napoli "Federico II", Naples, Italy

[3]Department of Engineering, Università della Campania "Luigi Vanvitelli", Aversa, Caserta, Italy

Correspondence
A. Formisano, Department of Engineering, Università della Campania "Luigi Vanvitelli", Aversa, Caserta 81031, Italy.
Email: Alessandro.Formisano@Unicampania.it

Abstract

Indirect lightning strikes hitting near photovoltaic installations are much more frequent than direct hits, and can generate overvoltage in their electric circuitry. The authors developed a method to estimate the induced overvoltage on single photovoltaic modules. Using a model of the whole array also including Inter-Module Coupling Mechanisms (IMCMs), a new approach to estimate overvoltage induced on full arrays is presented in this paper. The procedure first estimates lumped parameters, modelling either the coupling between the lightning channel and each module in the array or between each couple of modules in array. Several circuital simulations are then run using suitable equivalent circuits. The aim is to consider different array configurations and groundings schemes. This allows extracting the most relevant configuration parameters influencing overvoltage/overcurrent. Results show that the groundings scheme impacts negligibly, but the single module electric stress is decreased by 35% in the case of ungrounded configurations. Among the considered array configurations, the honey-comb and total cross-tied showed the smallest impact on overvoltage. Statistical analysis on random LC tortuous geometry leads to a non-negligible rise of overvoltage peak values, up to 24%. Finally, the relevance of different IMCMs is analysed, showing a strong impact just on frame-ground voltages and currents.

1 | INTRODUCTION

Lightning is one of the major threats to photovoltaic (PV) systems, due to their typically unsheltered installations. This problem is getting more and more relevant as installed systems with larger areas are getting common in response to the increased PV energy demand [1–4]. While direct lightning strikes (LS) are well studied phenomena, and suitable countermeasures are available [2, 5], the indirect LS, hitting near the PV system, are more frequent than the previous ones, yet less studied in their effects. As a matter of fact, indirect strikes proved to induce extremely high overvoltages in the PV circuitry [6, 7]. These overvoltages are transitory phenomena that can damage the insulation of the PV equipment, such as the PV modules [2, 8, 9], the inverters, the batteries etc. [10–13]. Therefore, a method for the simulation of such transients can help in the design of suitable protections.

Most of the studies about LS effects in the literature encompassed direct LS on small-size PV arrays [3, 6, 14–21]; some of them were devoted to medium or large-size PV arrays [22–24], but only few analysed lightning-induced overvoltage transients at the AC or DC side of grid-connected PV systems [4, 25–35]. Using different electromagnetic (EM) analysis for the DC side [36], these works assessed the lightning-induced voltages in the loops formed by the internal circuit of the PV module or the wiring of the PV array. From these analyses, the essential factors and their effects on the induced voltage were identified, such as: (i) the design of the lightning protection system and of the array grounding [4, 14–16, 21–24, 29, 34, 35]; (ii) the LS spot [14–18, 23, 24, 26, 32]; (iii) the lightning current flow in the metallic support mesh [4, 6, 14, 17, 22, 23]; (iv) the lightning current amplitude and waveform [4, 16, 21, 22, 24, 32]; (v) the soil resistivity and permittivity [3, 16, 21–24, 31, 32, 34]; (vi) the LC geometry [32], (vii) the array configuration [29]; (viii) the terrain geometry [31, 32].

To the authors' best knowledge, most of the previous studies on PV arrays are based on over-simplified models. In general, they are not able to provide a complete and systematic evaluation of the lightning-induced overvoltage due to the poor modelling of the single module coupling mechanisms (SMCMs)

between the internal circuit and its metallic frame. The main mechanisms can be related to the capacitive coupling (CC) [1, 8, 12, 14, 15, 37–40], the inductive coupling (IC) [1, 8, 12, 22, 27, 41, 42] and the ground coupling (GC) [40, 43, 44]. Moreover, a review of the PV literature discloses that quite a few papers [1, 8, 12, 22, 31, 32, 41, 42, 45] evaluated the overvoltage induced by nearby LS, frequently using a vertical straight segment to model the LC [31, 41, 45]. Even in the few available studies on indirect discharges, very little attention was paid to the analysis of medium-size PV arrays occupying large open areas [32, 41, 45].

PV arrays are formed by strings of series-connected modules, shunted across each other to create series-parallel (SP) configurations [46]. The SP drawback is the high impact that a particular mismatching can have on the overall array performance. Therefore, the geometry of the configuration is one of the most profitable degrees of freedom in the array design to alleviate the mismatching in parameters, operating conditions, and security threats [47]. Total cross-tied (TCT), honey-comb (HC) or bridge-linked (BL) are three widely adopted regular configurations [48]. A number of studies analysed the impact of partial shading on different PV array configurations (SP [47, 49–52], TCT [47–54], BL [47–53] or HC [47, 51–53, 55, 56]). A few also analysed the influence of other mismatching parameters [55], but as far as we know, none presented an assessment of the behaviour of nearby LS over voltages for different PV array configurations.

The available literature about the impact of nearby LS on large PV systems is scanty. Furthermore, the modelling of Inter-Module Coupling Mechanisms (IMCMs), both CC and IC, and of module grounding coupling mechanisms (MGCM), and its extension to the whole PV array, is relatively new [12]. To the best of our knowledge, no study has yet reported on the influence of these mechanisms.

Ref. [1] proposed a prompt 3D semi-analytical method, able to compute the differential and common mode voltages induced by tortuous LC hitting nearby PV module in no-load conditions. The module model was improved in [8] including the high-frequency effects and the ground coupling. Starting from these studies, a preliminary study on the EM couplings between neighbouring modules [12] yielded the knowledge of the related lumped parameters of the couplings.

We propose here a model suited to deal with the whole PV array, including, as required, the IMCMs and MGCMs. The proposed approach is divided in two steps: first, the 3D semi-analytical models are used to estimate the lumped parameters describing the couplings between: (i) the LC and either the module circuitry or the frame; (ii) the circuitry and the frame of the single module; (iii) the adjacent modules; (iv) each module's circuitry and the Mounting System (MS). The circuits corresponding to different array groundings and configurations (including the lumped parameters for the above introduced coupling mechanisms) are then simulated using circuital simulators. The computed overvoltage in different points of the equivalent circuits (or equivalently in different points of the arrays) represent the outcome of the analysis. Taking advantage of the gathered data, we finally analyse some key factors influencing this phenomenon in medium-size PV array of 8 × 4 modules.

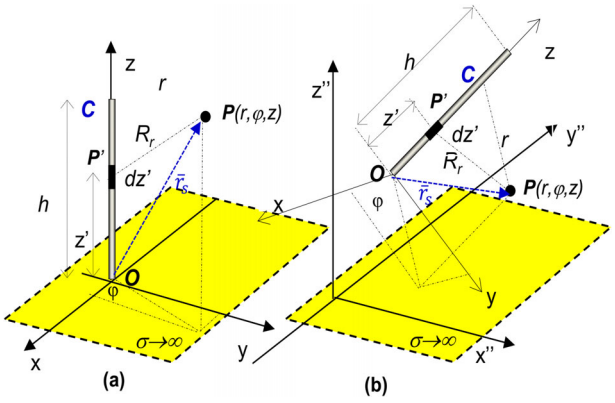

FIGURE 1 (a) Vertical discharge channel segment; (b) Arbitrarily oriented discharge channel segment

Internal design issues, such as the array grounding and configuration, and external conditions, such as the LC geometry and the LS spot, are considered. In addition, the relevance of the IMCMs and MGCMs is assessed.

The rest of the paper is organized as follows. Section 2 introduces the model for the coupling between the LC and a single PV module. The model of the coupling mechanisms for the whole PV array are detailed in Section 3. Section 4 briefly introduces the array configurations considered in the study. Section 5 defines the simulation design and experimental set-up. Finally, Section 6 qualitatively and quantitively investigates the influence of some key factors that impact the overvoltages in a case study for a PV array. Concluding remarks are in Section 7.

2 | EM MODELLING OF COUPLING PHENOMENA

Computing the induced voltage on a single PV module by an indirect LS requires three basic steps, that is, the representation of lightning current, the computation of lightning EM field and the modelling of the coupling between the EM field and PV module. As the attention in this research is mainly focused on the overvoltage in different points and for different configurations and groundings of the PV array equivalent circuits, we present here only the basic elements of the EM models used to estimate the equivalent circuit (lumped) elements, and the circuits themselves, for single modules. More details can be found in [1, 8, 12].

2.1 | EM field from lightning current

Current in real LCs follows tortuous paths from clouds to ground. Consequently, in the adopted model [1] the LC is represented by several randomly oriented segments, starting from an infinitely conducting ground in proximity of a PV array and raising towards the clouds. Parameters describing the channel geometry are chosen according to the data on natural flashes. Figure 1a,b shows the relevant quantities used in the computation of fields from the LC.

As described in detail in [1], the first step involves the calculation of the step response, that is the calculation of the magnetic vector potential $\boldsymbol{A}(r_s, t)$ produced by a vertical channel starting from the ground and travelled by a step current of amplitude I_0 and velocity v:

$$i(z', t) = I_0 \left[u\left(t - \frac{z'}{v}\right)\right] [u(z') - u(z' - h)] \quad (1)$$

where u is the Heaviside step function, h is the height of the lightning channel and z' is the local coordinate on the channel (see Figure 1a). The vector potential $\boldsymbol{A}(r_s, t)$ is directed along the z-axis and is independent on the azimuthal coordinate φ:

$$\boldsymbol{A}(r_s, t) = \frac{\mu_0}{4\pi} \int_0^h \frac{I_0 u\left(t - \frac{R_r}{c} - \frac{z'}{v}\right)}{R_r} dz' \hat{\boldsymbol{i}}_z \quad (2)$$

In (2) μ_0 is the vacuum permeability. The involved geometrical parameters are represented in Figure 1. The method of images is then adopted to consider the presence of a perfectly conducting ground: the contributions of the "direct" channel segment and of its "mirror" are summed up to provide the resulting vector potential.

This simple analytical formula for the vector potential can also be used for each arbitrarily oriented segment composing a tortuous LC: the calculations are made by using a proper local coordinate system (Figure 1b) originating from the starting point O of the generic channel segment, and whose z-axis is coincident with its axis. A suitable coordinate transformation is required at each segment to combine different contributions in all space. Also in the case of a tortuous channel, the resulting vector potential is calculated by adding the contributions of the "direct" segment and of its corresponding "image".

Once the vector potential produced by a step current has been obtained, the calculation of the potential due to a generic current $i(t)$ propagating along the channel is performed by convolution summation, according to Duhamel's theorem [56]. The generic lightning current $i(t)$ is supposed to propagate without attenuation or distortion at constant speed v, equal to 1/3 of the speed of light c in vacuum. In the following, the current waveform is expressed by the Heidler's equation according to IEC 62305-2 [57]:

$$I_0(t) = I_{max} \frac{(t/\tau_1)^n}{1 + (t/\tau_1)^n} e^{-\frac{t}{\tau_2}} \quad (3)$$

where I_{max} is the peak value of the lightning current, t is the time, τ_1 is the rise time constant, τ_2 is the delay time constant, and n is the power factor of current rise speed. Typically, τ_1 is in the range of a few ms, while τ_2 is in the range of hundreds of ms, and $n = 10$.

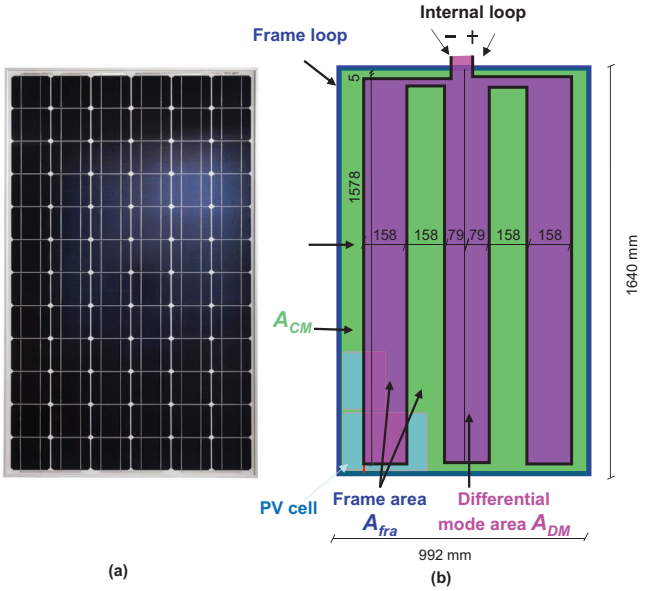

FIGURE 2 (a) Picture of a real PV module; (b) Adopted geometric model

2.2 | Coupling between PV module and LC

Figure 2a shows a picture of a real PV module, with the PV cells and their connections, while Figure 2b shows its corresponding schematic representation. The coupling between the LC and the single PV module is modelled as follows: the vector potential $\boldsymbol{A}(r_s, t)$ is line integrated along the inner circuitry of each module (black line in Figure 2b, encircling purple area) and along the boundaries of the aluminium protection case (blue lines, encircling green area) in order to obtain the magnetic flux Φ_{DM} linked across the area $\mathcal{A}_{DM}$ and the magnetic flux Φ_{fra} linked across the area $\mathcal{A}_{fra}$. The magnetic fluxes Φ_{fra} and Φ_{DM} are then time differentiated to evaluate the induced voltage (V_{mod}) on the PV inner circuit, and the induced voltage (V_{fra}) on the frame, which are represented in the equivalent circuit of Figure 3 as independent voltage sources (full details are given in [1, 8]). This approach was validated against experimental data available in [7]. Once the induced voltages are available, it is possible to set up the equivalent dynamic circuit of lumped elements, as shown in Figure 3. This circuit also includes the elements that model the SMCMs [1] and the dynamic and insulation parameters of the module. Thus, for the lightning transient study in this paper, the dynamic PV single-diode model is adopted. Details for deriving the RC equivalent circuit that characterize the AC dynamic model of a PV module can be found in [8]. The modelling of the PV module electrical insulation (insulation resistance and capacitance) was already defined in [43]. It consists of a leakage capacitance ($C_{p\text{-}lek\_mod}$), a series insulation resistance ($R_{s\text{-}lek\_mod}$), and a parallel insulation resistance ($R_{p\text{-}lek\_mod}$).

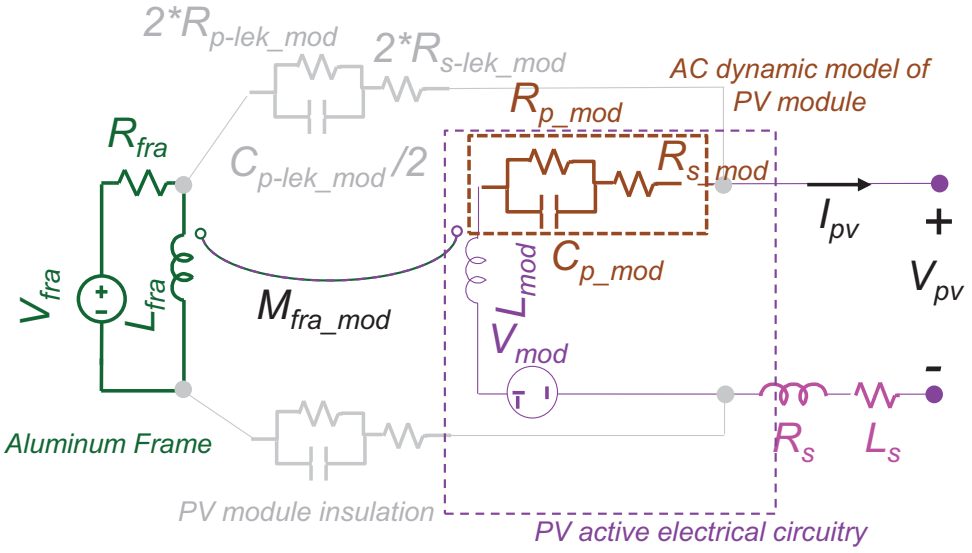

FIGURE 3 Equivalent circuit for a PV module under the coupling of LC including SMCMs and dynamic/insulation parameters

3 | MODELLING OF COUPLINGS FOR THE PV ARRAY

3.1 | Coupling mechanisms for PV inter-module

When modules are arranged into an array, it is reasonable to expect EM couplings between adjacent units. The most relevant IMCMs are: (i) displacements currents between neighbouring frame sides (CC) and (ii) induced voltages due to linked magnetic flux from currents in neighbouring frames or internal circuitries (IC). The first ones are modelled using parasitic capacitances, while the second ones using parasitic mutual inductances in the frame or the module circuits. The related lumped parameters are shown in Table 1, while the subcircuits considering the couples of modules neighbouring along long and short sides are illustrated in Figure 4, where 5 modules are "extracted" from a larger PV array, and each module is modelled using the (sub-)circuit in Figure 3, hidden inside the dashed boxes.

In the exemplifying figure, the module #2.2 (from the string #2) is connected with the two modules #2.1 and #2.3 from the same string, and with two modules of different strings, namely #1.2 and #3.2, highlighting the most significant couplings.

The most relevant inter-modules CC is the stray capacitance between adjacent frames. In this case, the expression per unit length for strip capacitors is adopted [58]:

$$C_{strip} = \varepsilon_0\, b\left[1 + \frac{1}{\pi b}\left(\log\frac{\pi}{b} + 1\right)\right]\left(\frac{F}{m}\right) \tag{4}$$

where b is the ratio of the strip's height to the distance between strips. The estimates for both long and short frame sides were successfully validated against 3D FEM models of two neighbouring modules [12].

The IC elements, thanks to the linearity assumption for all materials, can be computed using a semi analytical approach, like the one exposed for the LC to module coupling, where the magnetic vector potential from the "sources" is line integrated along the target circuit [59]. The only difference is in the geometry of currents induced in the frames, that we assume as a parallel connection of square "equivalent" coils.

3.2 | Grounding-module coupling mechanisms

The MGCM between frame and ground coupling was modelled using a parallel resistive capacitive connection (R_{fra_gnd}, C_{fra_gnd}, Figure 4). The resistive part was modelled using typical values from the braided wires used for these connections (in the order of mΩ), and the capacitive part being modelled by the capacitance of a tilted plate over a conducting plane [60]:

$$C_{gnd} = \frac{\varepsilon_0}{2\alpha}\log\left(1 + \frac{l}{h\cot(2\alpha)}\right) \tag{5}$$

where l is the plate width (the same as the PV module), h is the height of the lowermost point of the module to ground on the MS, a is the module angle to ground, and the conducting plane is considered by the image theory.

3.3 | Mounting system

The MS for a PV array is generally made of aluminium alloy, low-carbon steel or stainless steel. Two types of MS are commonly used according to the number of mounting legs, namely, one-leg structures and various-leg structures. The MS grounding system consists of a series of metallic rods buried in an

TABLE 1 Main data for the IMCMs

(a) Stray capacitances, CC

Coupled elements (adjacent frames)	Illustrative picture
Long side ($C_{fra\_fra\text{-}lng}$) Short side ($C_{fra\_fra\text{-}shrt}$)	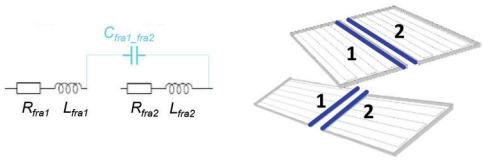

(b) Stray inductances, IC

Coupled elements (depending on the position)	Illustrative picture (long position)
Adjacent frames ($M_{fra\_fra\text{-}shrt}$ **or** $_{lng}$) Adjacent inner circuitries ($M_{mod\_mod\text{-}shrt}$ **or** $_{lng}$) Inner circuitry and adjacent frame ($M_{fra\_mod\text{-}shrt}$ **or** $_{lng}$)	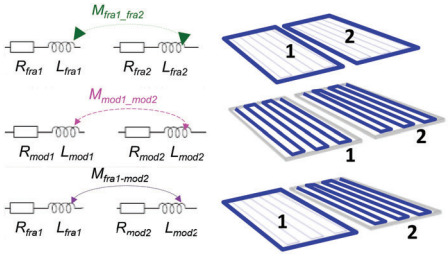

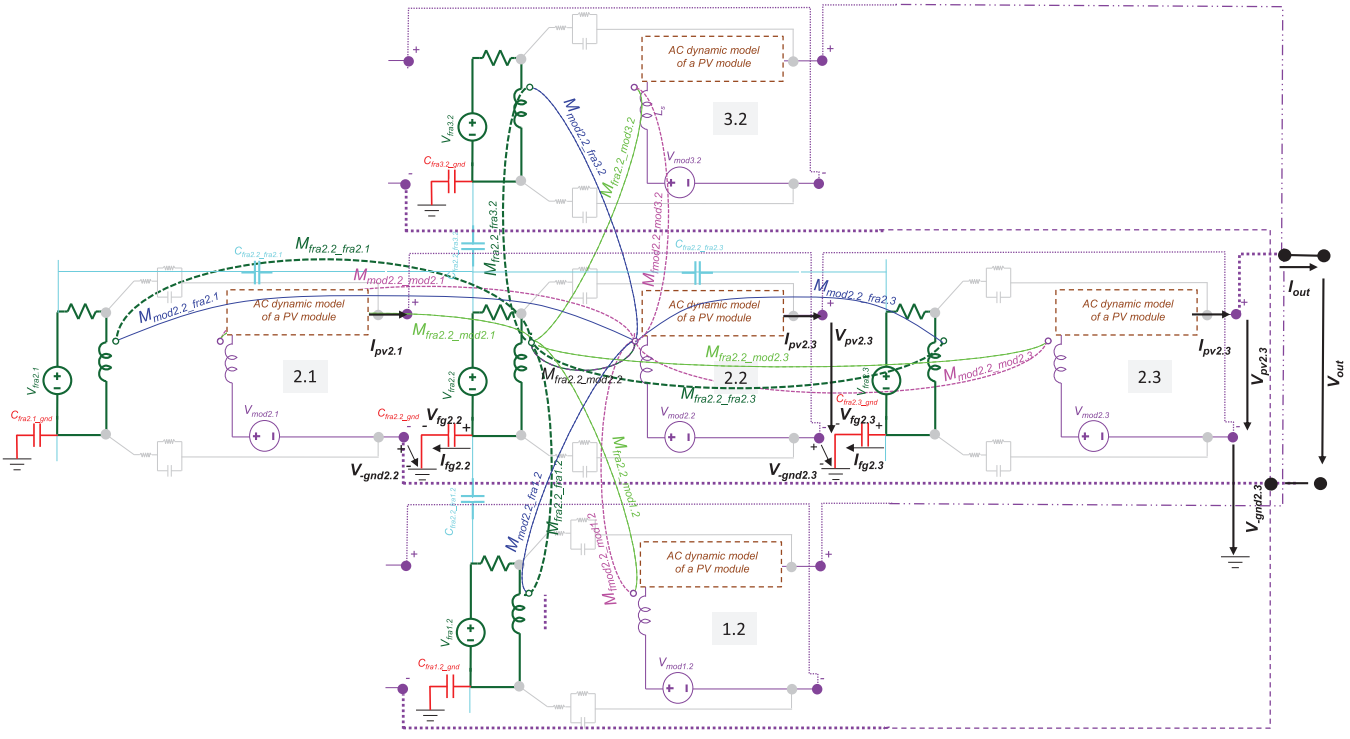

FIGURE 4 A schematic layout of a subcircuit with just 5 modules from a larger PV array, illustrating the inter-module elements of CC and IC

appropriate depth in earth. This metallic structure provides a near-zero impedance. Although no standard recommends which leg should be connected to the grounding grid [2], in this study all the legs of the MS are connected to the grounding rods to achieve equipotential bonding. Since a nearby LS causes only a negligible lightning current flow at the ground electrodes, a througout study of the grounding impedance was not necessary. The impact of the capacitive coupling with the metallic

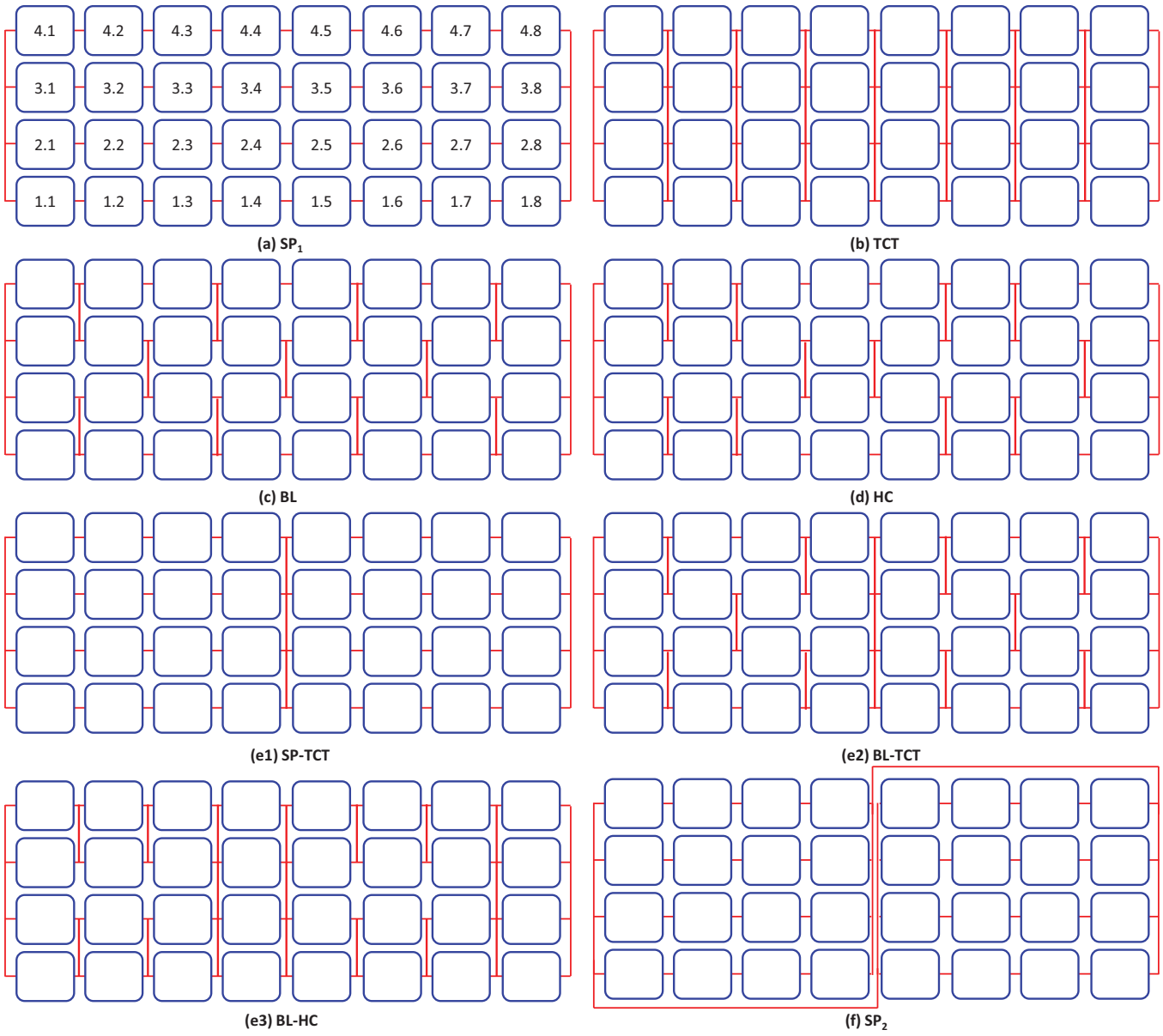

FIGURE 5 (a,f) Schematic wiring for an 8 × 4 PV array: configuration SP; (b) TCT; (c) BL; (d) HC; (e1–e3) hybrid: the two hybridized configurations are indicated in the figure

structures was assessed using the 3D FEM model described in Section 2.1. Assuming all parts are made of aluminium and electrically connected, we found that their impact is less relevant than the one of the frames coupling, so we neglected it.

4 | PV ARRAY CONFIGURATION

Figure 5 shows the schematic wiring of an 8 × 4 module array in the configurations analysed in the case study amongst those presented in Section 1. Figure 5a shows an SP configuration, which is the most widely adopted one [46] thanks to its ease of construction, low cost, and lack of redundant connections. The TCT configuration (Figure 5b) is derived from the SP configuration by connected crossties across each row of the modules [47, 52, 53, 61]. In this configuration, the voltage across each row is equal and the sum of current across each column is equal. For the BL configuration there is a bridged unit with four modules (Figure 5c). Two modules in a bridge are connected in series and then they are connected in parallel. Bridges are linked via cross ties [47, 52, 55]. The HC configuration [48, 61, 62] (Figure 5d) is a modified version of the BL configuration and its bridge size is variable. All the PV modules are interconnected like the hexagon shape of the HC architecture. The HC configuration has a greater number of electrical connections between the PV modules compared to the SP configuration, and has a smaller number of series connections compared to the TCP configuration.

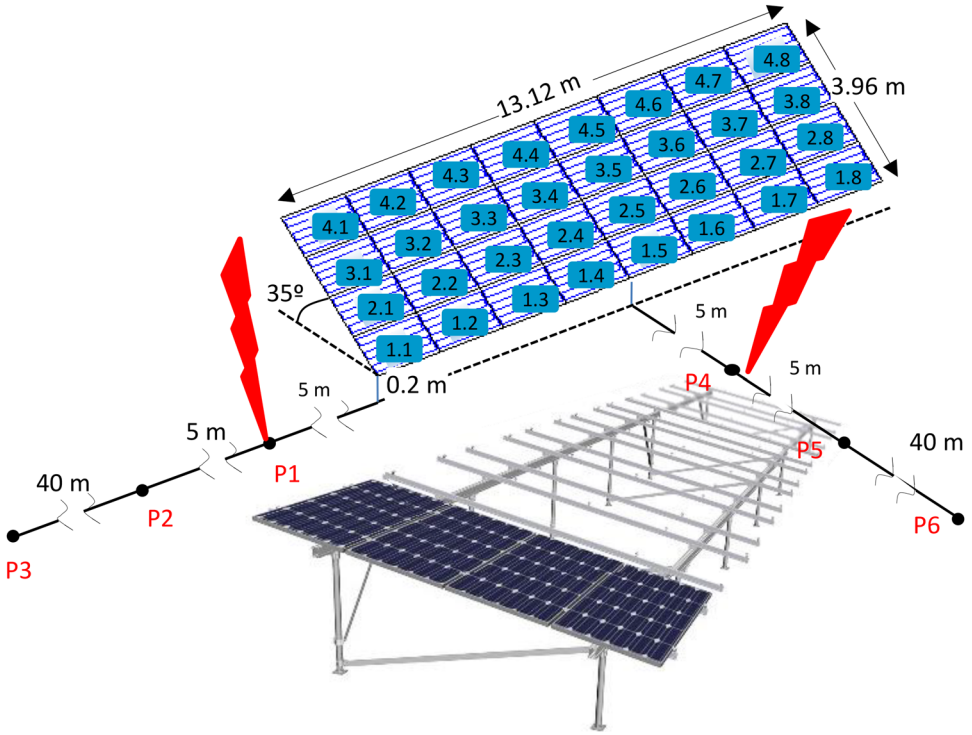

FIGURE 6 Configuration for the 8 × 4 PV module array. Twelve-leg mounting structure

Three hybrid PV array configurations were also proposed in [63, 64], which were SP-TCT, BL-TCT and BL-HC. They were derived from SP, HC and BL configurations by increasing their interconnection redundancy as illustrated in Figure 5e.

5 | SIMULATION DESIGN AND EXPERIMENTAL SET-UP

5.1 | Simulation setup

As mentioned above, a 3D semi-analytical method is used to estimate lumped coupling parameters. The method was developed by the authors and validated against 3D FEM computations [12]. Then, different circuits, each corresponding to a different grounding and connections configuration, are simulated using a MATLAB-based lumped circuit simulator.

TABLE 2 Coupling parameters between PV module and LC

Symbol	Physical effect	Typical value
R_{fra}	Resistance of the aluminium frame	1.3 mΩ
L_{fra}	Frame self-inductance	3.0 μH
L_{mod}	PV module self-inductance	2.3 μH
$M_{fra\text{-}mod}$	Mutual inductance between frame and module	2.6 μH
$R_{s\text{-}lek\_mod}$ ($R_{p\text{-}lek\_mod}$)	Series (shunt) insulation resistance of PV module between active circuitry and the frame	0.003 kΩ 0.38 kΩ
$C_{p\text{-}lek\_mod}$	Shunt capacitance between active circuitry and frame	180 nF
C_{p_mod}	PV module junction capacitance	1.36 μF
R_{p_mod} (R_{s_mod})	Series (shunt) PV module resistances, respectively	35.6 kΩ 0.807 Ω

5.2 | Test system description

The PV array is placed on a 35°-inclined twelve-leg stainless steel MS of 13.12 m in length and 3.96 m in width. The height at the front of a frame is 0.2 m from the ground, Figure 6.

This 8 × 4 module array can be considered a medium size one (common in the residential and commercial context) with an 8.64 kWp power from 32 commercial PV modules of 270 Wp [1]. Each module has 60 cells (6 × 10), all series connected (V_{oc}: 38.06 V, V_{mpp}: 30.90 V, I_{mpp}: 8.6 A). For convenience, the 32 modules were arranged either in 4 strings (V_{oc}: 913 V, V_{mpp}: 742 V, with 7 possible configurations: SP_1, TCT, BL, HC, SP-TCT, BL-TCT, BL-HC, Figure 5a–e) or in 8 strings (V_{oc}: 457 V, V_{mpp}: 371 V, with only SP_2 configuration). Bypass diodes and blocking diodes were omitted.

The technical data describing the SMCMs and the dynamic and insulation parameters of the single modules are reported in Table 2; their values are according to [1, 8].

Each module is assumed embedded in an aluminium frame; the length of the frame (long dimension) is 1.64 m, its width

TABLE 3 Main data describing the IMCMs

Coupled elements		Lumped parameter value
CC (adjacent frames)	Along long side	$C_{fra\_fra\text{-}lng}$= 40 pF
	Along short side	$C_{fra\_fra\text{-}shrt}$ = 20 pF
IC	Adjacent frames	$M_{fra\_fra\text{-}shrt}$= $M_{fra\_fra\text{-}lng}$ = 1.0 μH
	Adjacent inner circuitries	$M_{mod\_mod\text{-}shrt}$= $M_{mod\_mod\text{-}lng}$= 0.1 μH
	Inner circuitry and adjacent frame	$M_{fra\_mod\text{-}shrt}$ = $M_{fra\_mod\text{-}lng}$ = 0.3 μH

(short dimension) is 0.99 m, its height is 2 cm, and the inter-module distance is assumed to be 1 cm. Aluminium resistivity is σ_{al}= 105 S/m. These figures lead to the values of the parameters of the IMCMs reported in Table 3. The MGCM provided a capacitor C_{fra_gnd} of 3–7 pF, depending on the PV row in the MS.

6 | RESULTS

In this section, the reference case is firstly considered. Then a comprehensive assessment of the behaviour is performed with respect to some key factors that influence the overvoltages induced in the PV array by a nearby LS. Considered factors are design issues, such as the array grounding and strings arrangement, and external conditions such as the LC geometry and the LS spot distance. Furthermore, in such a framework, the relevance of the IMCMs and MGCMs are disclosed.

Waveforms and peak magnitude values are reported for each considered variable. The monitored variables are (Figure 4): (i) differential mode voltage of PV array (V_{out}); (ii) output current of PV array (I_{out}) (iii); differential mode voltage in PV module #i.j ($V_{pv\ i.j}$); (iv) output current of PV module #i.j ($I_{pv\ i.j}$); (v) voltage between negative terminal of PV module #i.j and ground ($V_{gnd\ i.j}$); (vi) voltage between PV frame of module #i.j and ground ($V_{fg\ i.j}$); (vii) current between frame of PV module #i.j and ground ($I_{fg\ i.j}$). The meaning of the quantities reported in the legends can be recognized from Figure 4.

6.1 | Reference case

As a reference case, we assumed the parameters for the AC (frequency) dynamic model of PV module according to [8], calculated at a frequency of 1 MHz, and in cloudy conditions (a 100 W/m^2-irradiation, low PV module insolation) when there are storms and nearby LS can occur. Maximum power point (MPP) condition was set as array voltage bias. Moreover, we considered a vertical LC with a first stroke waveform hitting at LS spots P1 and P4 (5 m away from the PV array, Figure 6). The SP configuration of the PV array was grounded at the negative output of array and all the IMCMs (CC and IC) together with the MGCM were considered.

The distance of the LS spots from the array, although not very likely, was chosen to highlight the effects of parameters' variation, which could have been negligible if larger distances were chosen. LS spot distance was anyway among the considered parameters, and its impact is investigated in Section 6.4.

Figures 7a–d and 8a–c report the voltages and currents induced for the whole PV array as well as for some relevant specific PV modules for the reference case and a striking spot at P1. Note that the output voltage V_{pv} available at the PV array terminal (Figure 7a) is due to the cumulative effect of induced voltages $V_{mod\ i1\text{-}8}$ throughout all the 8 modules of each string i (i = 1,…,4). Since the LS spot is on the left side of the array, as the considered module (Figure 8c) is the last in each row of the string and the row is located in the upper portion of the MS, the peak value of induced voltage is the smallest, and is attained later, even reaching negative values for modules located in more distant places of the MS. The output currents of PV modules follow a different pattern (Figure 8d); in each row of the MS (string), currents of modules are almost the same (expect currents flowing to ground), but a change in the peak value behaviour from positive to negative current values is observed when further increasing the distance.

Results in Figures 7c and 7d disclose that in common-mode, voltages up to some 2.40 kV (module #1.1) and induced currents up to 247.55 A (module #4.8) can be induced in a single module. From regulations [2, 65–67] that determine the surge withstand capability (SWC) of overvoltages in a PV module (in the interval 4–8 kV) as well as its current withstand (about 2 kA), it is reasonable to expect that the insulation does not fail in the PV module under the considered conditions.

Given that the negative terminal of the PV array is grounded and electrically located at the opposite side of the LS spot, the peak voltage of negative terminal to ground in each module increases as the spot gets closer to the module, either by the position within row (string) or by the localization of row in MS. Accordingly, the voltage in the module #1.1. (differential-mode, Figure 8a) can reach high values (−8.38 kV), leading to the breakdown of the PV module insulation [65–67]. Therefore, this differential-mode overvoltage is the most threatening.

Induced voltages in the module, frame to ground, and resulting currents follow a different behaviour depending on the specific location in the MS (Figure 8b,c). The results of low voltages and resulting low currents disclose that there are no threats to insulation breakdown.

When the results of LS spot P4 (centred to the MS) are compared with those of spot P1 (at the left side of the MS), the main difference appears in the differential mode voltages of the modules that almost always develop negative values for all of the modules in a string (Figure 9c) and therefore, a higher negative peak for the PV array is attained (Figure 9a). By contrast, in P1 the latter variable is lower since there is a positive and negative compensation of voltages between the modules of the string. This addition effect is augmented in the module currents (Figure 9d), and string currents. This generates an almost doubled output current in the PV array with respect

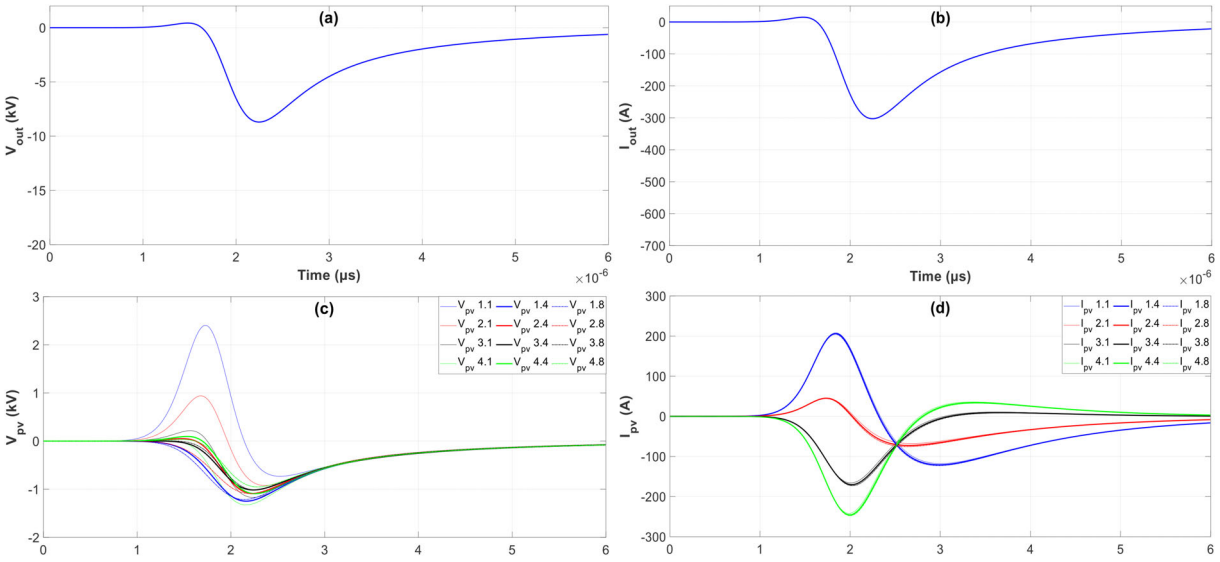

FIGURE 7 Reference case, voltages and currents induced, spot P1

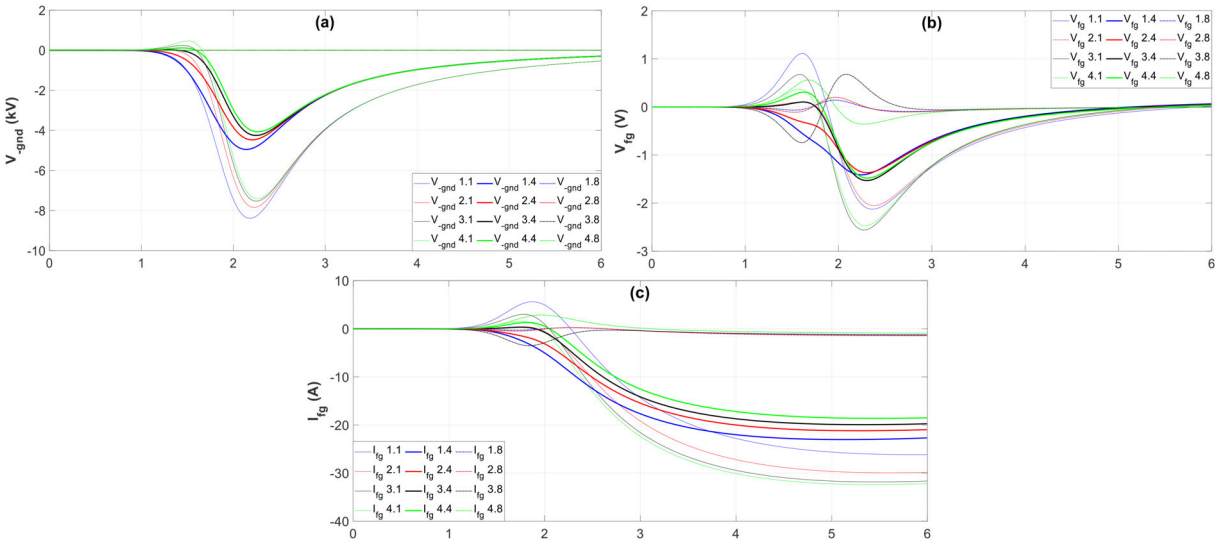

FIGURE 8 Reference case, voltages and currents induced, spot P1

to the corresponding P1 figure (Figure 9b). Also, due to the voltage accumulation effect, the negative terminal to ground voltage at each module increases (Figure 10a). For example, in the case of LS spot in P4, this figure reaches 15.19 kV in module #1.1, nearly doubling the value corresponding to the P1 spot case. Finally, relative changes in the voltages, frame to ground, and resulting currents appear in P4 versus P1, but insulation breakdown is not expected.

6.2 | Relevance of couplings in the PV array

To rank the relevance of the IMCMs and MGCMs, introduced in this study, the influence of each of them is separately assessed. For each mechanism, a relative variation of ±10% is considered to account for the uncertainty associated with the coupling modelling process. We also analysed the impact of the frame material, using a steel frame instead of an aluminium frame. The impact of the steel choice is quite low since the maximum decrease in the variables reaches about 4%, being 1% for most variables. The effects are computed and compared to the reference case and the base case (reference case without any coupling mechanism). Table 4 reports the peak magnitude values for the monitored variables when the LS spot is in P4.

The effect of the MGCM is extremely interesting; it significantly decreases the induced voltages of the PV frame to ground to much smaller values than to base case, namely 102% iof the reference case; also, it increases the current frame to ground that reaches up to 91% of the reference case. As for

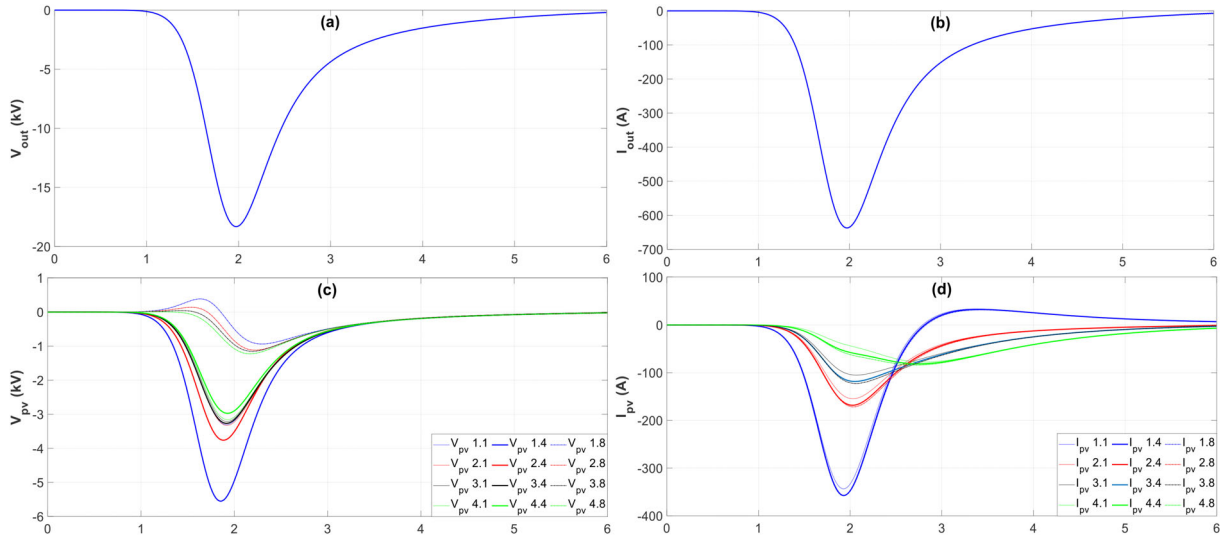

FIGURE 9 Reference case, voltages and currents induced, spot P4

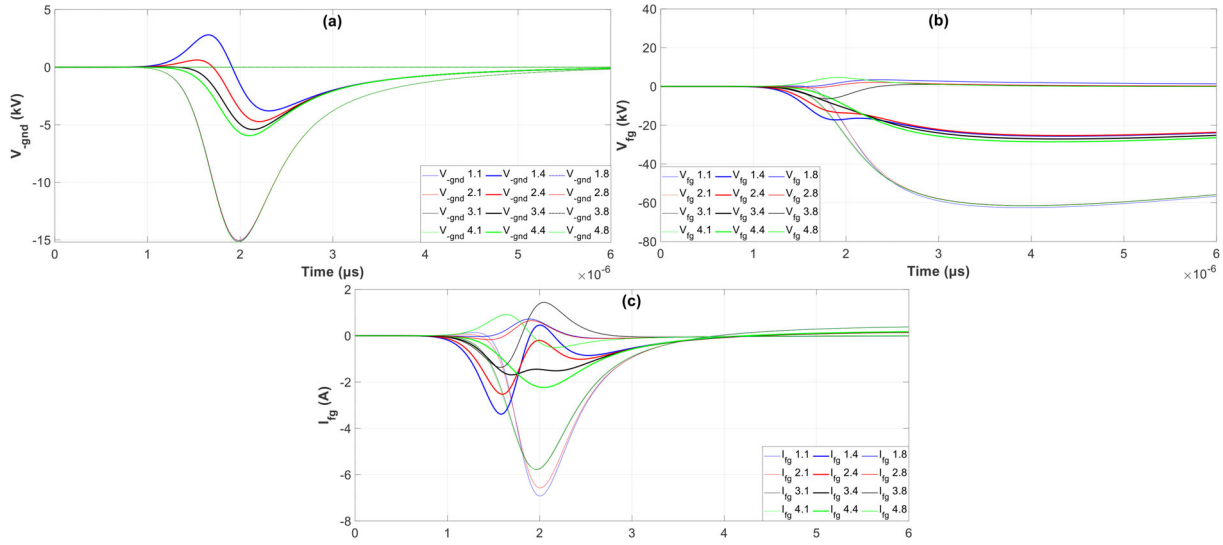

FIGURE 10 Reference case, voltages and currents induced, spot P4

TABLE 4 Relevance of couplings in the PV array, spot P4

	V_{out} (kV)	I_{out} (A)	$V_{pv(\#i,j)}$ (kV)	$I_{pv(\#i,j)}$ (A)	$V_{\text{-}gnd(\#i,j)}$ (kV)	$V_{fg(\#i,j)}$ (V)	$I_{fg(\#i,j)}$ (A)
Reference case	−18.30	−636.87	−5.54 (#1.4)	−359.76 (#1.5)	−15.18 (#4.1)	−62.54 (#1.1)	−6.92 (#1.1)
Base case	−20.18	−702.28	−6.14 (#1.4)	−303.81 (#1.8)	−16.69 (#4.1)	−23,372.8 (#1.1)	-1.35×10^{-5} (#1.1)
Base case, Steel	−20.05	−697.95	−6.02 (#1.4)	−292.20 (#1.8)	−16.63 (#4.1)	−20,232.6 (#1.1)	-3.31×10^{-5} (#1.1)
Base case + MGCM	−19.84	−690.71	−6.06 (#1.4)	−322.48 (#1.5)	−15.46 (#4.1)	−63.5 (#1.1)	−6.28 (#1.1)
+10%	−19.84	−690.71	−6.06 (#1.4)	−322.48(#1.5)	−15.46 (#4.1)	−57.7 (#1.1)	−6.28 (#1.1)
−10%	−19.84	−690.71	−6.06 (#1.4)	−322.48 (#1.5)	−15.46 (#4.1)	−70.4 (#1.1)	−6.28 (#1.1)
Base case + IMCM-CC	−20.14	−700.89	−6.13 (#1.4)	−305.80 (#1.3)	−16.65 (#4.1)	−19,351.7 (#3.1)	-3.57×10^{-5} (#3.1)
+10%	−20.14	−700.88	−6.13 (#1.4)	−305.91 (#1.3)	−16.65 (#4.1)	−19,280.5 (#3.1)	-3.53×10^{-5} (#4.1)
−10%	−20.14	−700.90	−6.13 (#1.4)	−305.67 (#1.3)	−15.65 (#4.1)	−19,442.6 (#4.1)	-3.60×10^{-5} (#3.1)
Base case + IMCM-IC	−18.82	−654.89	−5.68 (#1.4)	−337.12 (#1.8)	−15.65 (#4.1)	−18,558.0 (#1.1)	-3.82×10^{-5} (#2.3)
+10%	−18.75	−652.48	−5.65 (#1.4)	−339.03 (#1.8)	−15.59 (#4.1)	−18,424.0 (#1.1)	-9.82×10^{-4} (#1.1)
−10%	−18.88	−654.32	−5.70 (#1.4)	−335.25 (#1.8)	−15.68 (#4.1)	−18,680.3 (#1.1)	-3.87×10^{-5} (#1.1)

TABLE 5 Effect of the array grounding

	V_{out} (kV)	I_{out} (A)	$V_{pv(\#i.j)}$ (kV)	$I_{pv(\#i.j)}$ (A)	$V_{\text{-}gnd(\#i.j)}$ (kV)	$V_{fg(\#i.j)}$ (V)	$I_{fg(\#i.j)}$ (A)
P1, grounded -reference case-	−8.70	−302.74	2.40 (#1.1)	−247.55 (#4.8)	−8.38 (#1.1)	−32.39 (#4.1)	−3.79 (#1.2)
P1, ungrounded	−8.75	−304.61	2.40 (#1.1)	−243.42 (#4.4)	−5.03 (#1.1)	−16.85 (#4.8)	−2.75 (#1.2)
P4, grounded -reference case-	−18.30	−637.87	−5.54 (#1.4)	−359.76 (#1.5)	−15.18 (#4.1)	−62.54 (#1.1)	−6.92 (#1.1)
P4, ungrounded	−18.41	−640.48	−5.56 (#1.4)	−352.48 (#1.4)	−9.09 (#4.1)	−38.12 (#1.1)	−5.30 (#1.5)

TABLE 6 Effect of the lightning striking spot, reference case

	V_{out} (kV)	I_{out} (A)	$V_{pv(\#i.j)}$ (kV)	$I_{pv(\#i.j)}$ (A)	$V_{\text{-}gnd(\#i.j)}$ (kV)	$V_{fg(\#i.j)}$ (V)	$I_{fg(\#i.j)}$ (A)
P1	−8.70	−302.74	2.40 (#1.1)	−247.55 (#4.8)	−8.38 (#1.1)	−32.39 (#4.1)	−3.79 (#1.2)
P2	−8.63	−300.45	−1.16 (#2.2)	−99.16 (#3.8)	−7.54 (#1.1)	−34.33 (#3.1)	−2.72 (#1.2)
P3	−8.08	−281.24	−1.12 (#2.1)	−87.67 (#4.8)	−6.98 (#1.1)	−34.43 (#3.1)	−2.35 (#3.1)
P4	−18.30	−637.87	−5.54 (#1.4)	−359.76 (#1.5)	−15.18 (#4.1)	−76,20 (#1.1)	−6.92 (#1.1)
P5	−15.03	−523.11	−2.59 (#1.2)	−253.65 (#1.8)	−12.73 (#4.1)	−54.09 (#1.1)	−4.99 (#1.1)
P6	−12.40	−431.56	−1.83 (#1.1)	−188.11 (#1.8)	−10.65 (#4.1)	−47.36 (#1.1)	−3.88 (#1.1)

the change of the remaining variables, this resulted in an overestimation of about 8%, except for module currents that get an underestimation of 10%. Note that the assessment on this coupling mechanism impacts only on the ground voltage, while the ground current is not influenced.

The impact of IMCM-CC is almost null as compared with the base case except for the frame to ground variables. However, the high/low values of such variables nullify any conclusion. The change assessment does not disclose influence on any variable. This mechanism, taken individually, is irrelevant.

The impact of IMCM-IC moves the results away from the base case and towards the reference case. Thus, this coupling leads to an improvement of about 7% regarding the base case for most variables, except for the module current and frame variables, so that it stands at an overestimation of just about 3% in these variables to the reference case. The change assessment is bounded by 1%.

6.3 | Effect of the array grounding

PV array grounding is not always required [2]. From the personnel safety viewpoint, floating configurations are safer than grounded configurations. The opposite case occurs when considering the lightning protection viewpoint [2]. Thus, both viewpoints are weighted in this section. To this aim, the reference case (grounded PV array) is compared with the ungrounded configuration for both LS spots P1 and P4, see Table 5.

In the "grounded" case we assumed that each pillar in the PV array support penetrates 1 m below the ground surface, and all pillars are connected by a large aluminium ribbon, 0.5 m below the ground level. The impact of the grounding configuration on induced voltages and currents was usually quite small. A marginal increase/decrease of about 1% could be observed in voltages and currents (both for the whole array and for the single modules) for the ungrounded configuration with respect to the grounded one. However, the removal of the direct current flow path to ground substantially changes the variables related to ground. As an example, the module voltage from negative pin to ground decreases more than 35% with respect to the grounded configuration. The same occurs for the frame voltage and current, arriving at a reduction of about 35–95% and 37-30%, respectively, depending on the LS spot position. This reduction of EM stress on the single modules makes the breakdown of its insulation less likely. So, this configuration constitutes an array design measure to alleviate the threat from overvoltages induced by nearby LS.

6.4 | Effect of the LS spot position

To assess the impact of the LS spot position, six different strikes hitting on the ground were considered for the reference case, namely at a distance of 5, 10 and 15 m away from the MS, 3 spots on the left of MS and 3 spots centred on the MS (see Figure 6). Two cases (namely, P1 and P4) had already been introduced in the previous discussion to assess the impact of LS spot position on some relevant variables. The analysis is now completed in a systematic way (see Table 6).

The nearer the LS spot position is to the MS, the larger are the peak values shown in overvoltages. For example, the overvoltages induced when considering spots P1 or P4 are much larger than those induced when considering the spots P2 or P5. Nonetheless, distance plays a moderate role. Thus, the voltage and current induced in the whole array decrease linearly with the distance, but with different coefficients (e.g. 1/2 for spots on the left of MS and 1/3 for spots in centred locations). In contrast, the voltage induced in single modules decreases linearly with distance. Finally, the remaining variables decline with

TABLE 7 Effect of the PV array configuration

		V_{out} (kV)	I_{out} (A)	$V_{pv(\#i,j)}$ (kV)	$I_{pv(\#i,j)}$ (A)	$V_{gnd(\#i,j)}$ (kV)	$V_{fg(\#i,j)}$ (V)	$I_{fg(\#i,j)}$ (A)
Spot P1	SP -reference case-	−8.70	−302.74	2.40 (#1.1)	−247.55 (#4.8)	−8.38 (#1.1)	−32.39 (#4.1)	−3.79 (#1.2)
	TCT	−8.64	−300.73	**−1.31 (#3.5)**	1408.7 (#1.1)	**−7.67 (#1.1)**	−32.75 (#4.1)	−3.49 (#3.2)
	BL	−8.65	−301.21	−1.42 (#3.3)	1065.9 (#1.1)	−7.96 (#1.1)	−31.46 (#4.1)	−3.39 (#1.2)
	HC	**−8.51**	**−296.33**	−1.61 (#2.3)	929.94 (#1.1)	−7.82 (#1.1)	**−30.37 (#4.1)**	−3.54 (#1.2)
	SP-TCT	−8.74	−304.39	2.09 (#1.1)	436.28 (#1.2)	−8.29 (#1.1)	−32.65 (#4.1)	−3.65 (#1.2)
	BL-TCT	−8.63	−300.39	−1.36 (#1.3)	1058.7 (#1.1)	−7.91 (#1.1)	−32.19 (#4.1)	**−3.38 (#1.2)**
	BL-HC	−8.64	−300.95	1.40 (#1.1)	973.06 (#1.1)	−7.90 (#1.1)	−32.04 (#4.1)	−3.53 (#1.2)
	SP2	−3.51	−122.43	1.95 (#1.1)	−533.02 (#4.4)	−3.80 (#2.5)	−19.31 (#2.5)	2.14 (#1.2)
	SP -reference case-	−18.30	−636.87	−5.54 (#1.4)	−359.76 (#1.5)	−15.18 (#4.1)	−62.54 (#1.1)	−6.92 (#1.1)
Spot P4	TCT	−17.77	−618.50	**−4.26 (#1.3)**	−1604.10 (#1.4)	**−14.64 (#1.1)**	−61.05 (#1.1)	−6.66 (#1.1)
	BL	−18.14	−631.24	−5.40 (#1.4)	−714.64 (#1.3)	−15.08 (#1.1)	−61.09 (#1.1)	−6.94 (#1.1)
	HC	**−17.73**	**−617.03**	−5.23 (#1.4)	−523.86 (#1.5)	−14.65 (#1.1)	**−59.94 (#1.1)**	−6.60 (#1.1)
	SP-TCT	−18.30	−636.80	−4.77 (#1.4)	−931.45 (#1.3)	−15.71 (#1.1)	−63.58 (#1.1)	−7.07 (#1.1)
	BL-TCT	−18.01	−626.94	−4.67 (#1.3)	−1470.00 (#1.3)	−15.05 (#1.1)	−61.55 (#1.1)	−6.89 (#1.1)
	BL-HC	−17.70	−616.10	−4.58 (#1.4)	−1617.61 (#1.3)	−14.73 (#1.1)	−61.34 (#1.1)	**−6.63 (#1.1)**
	SP2	−7.30	−254.15	−5.78 (#4.4)	2060.30 (#4.4)	−7.30 (#1.5)	−26.76 (#1.1)	−4.13 (#1.5)

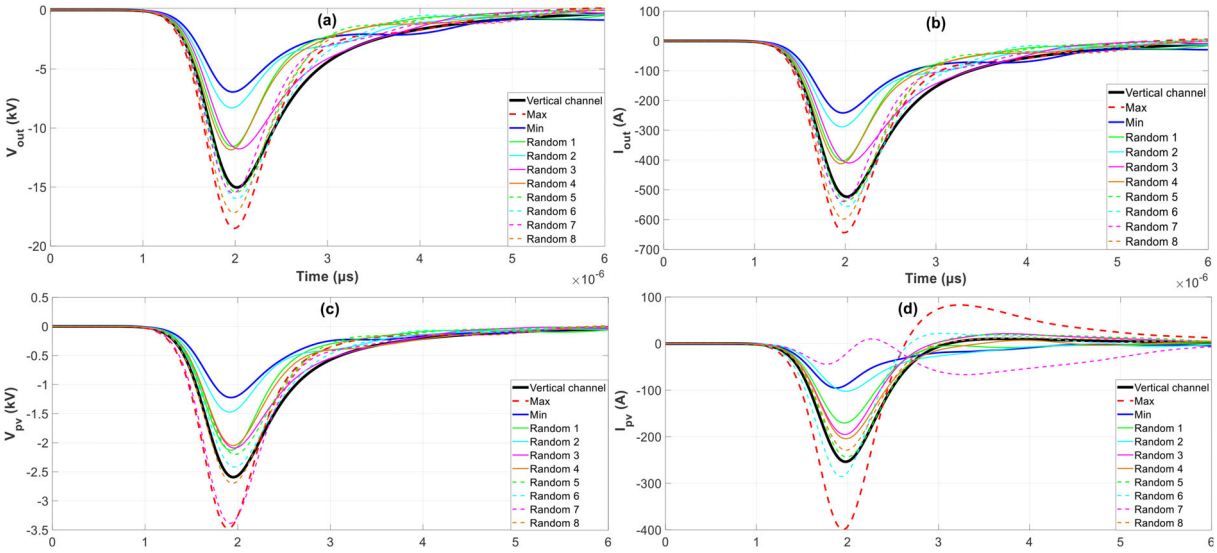

FIGURE 11 Effect of the LC geometry

a coefficient equal to 2 with respect to the distance. Therefore, it is evident that the centred or off-centre location of the lightning striking spot regarding the MS plays a primary role in the assessment of the EM stress on the PV modules/array. The closer the LC hits the centre of the MS, the more relevant is the effect of distance.

6.5 | Effect of the PV array configuration

Array configuration can be one of the most profitable degrees of freedom in the design to alleviate the overvoltages due to nearby LS. In this section, we focus on the performance of the seven configurations previously mentioned at spots P1 and P4 (Table 7) namely, SP, TCT, BL, HC, SP-TCT, BL-TCT, BL-HC.

Focusing hereafter on LS spot P1, the HC configuration produces the highest drop in voltages and currents for the whole array, about 3%. Furthermore, it generates the maximum reduction of frame to ground voltages (about 7%). Nonetheless, the least yet non-negligible frame to ground current is provided by the hybrid configuration BL-TCT, providing an 11% drop with respect to the reference case. However, for spot P4 this is not the case, and the BL-HC configuration, hybrid based on HC, proves again its superiority. The TCT configuration provides the

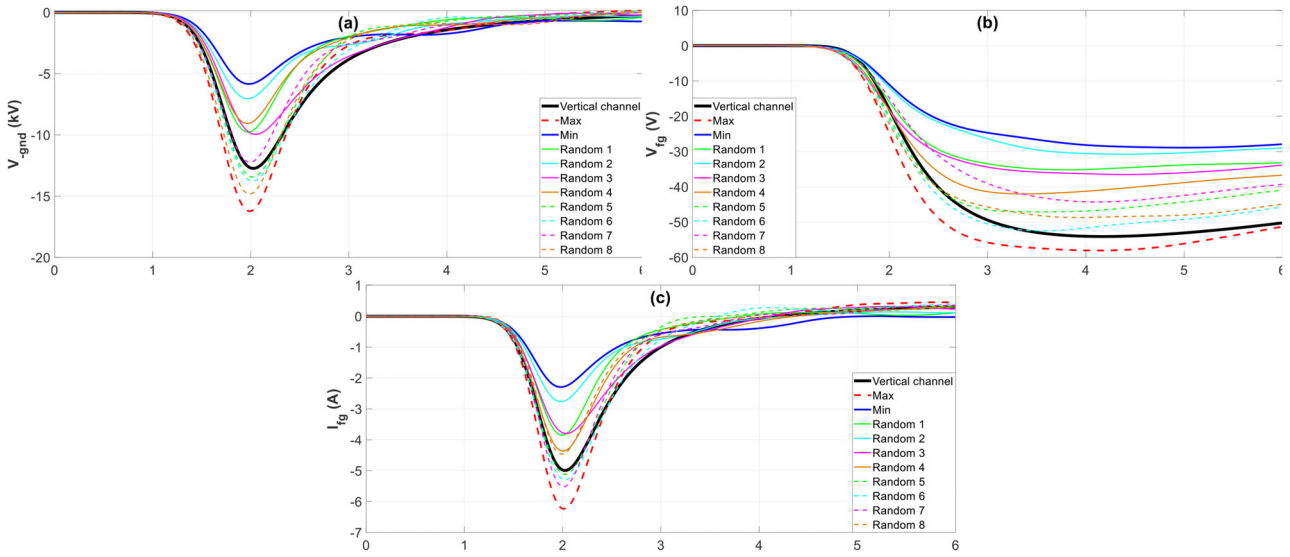

FIGURE 12 Effect of the LC geometry, continued

highest decrease for the module voltage in common mode, up to 45%. However, as all modules are cross connected, this entails that the module current achieves a dangerous peak in module #1.1 (1408.7 A), as there is an increase of 560% regarding the reference case. Moreover, this configuration outperforms the other configuration when voltage from negative to ground is assessed; more than a 7% reduction.

It is important to note that SP2 configuration generates the lowest voltages, with the currents bounded to suitable values. Therefore, when higher voltages are possible in the design stage, this configuration is preferred.

The only relevant fact from the results at spot P4 is that the peak voltage from negative to ground is generated by SPTCT instead of SP configuration (reference case).

6.6 | Effect of the LC geometry

To assess the impact of a tortuous LC, a statistical analysis using 100 randomly generated LC paths is performed. Example waveforms for 8 different LC's hitting at the LS spot P5 are reported in Figures 11a–d and 12a–c, whereas the averages, standard deviations, minimum and maximum values are reported in Table 8. Note that the vertical strike corresponds to reference case.

From the statistical analysis, it can be observed that tortuosity leads to a non-negligible rise in the peak values in the variables, influencing both currents and voltages, achieving up to 24% for most variables, except for the voltage (34%) and current (57%) in single modules at the worst locations #1.2 and #1.8, respectively. The standard deviation values suggest that the statistical variability of the LC geometry cannot be neglected when dimensioning the lightning protection system. Accordingly, the LC geometry plays a leading role in the assessment of the EM stress on a PV array. The hypothesis of a vertical straight strike channel may lead to underestimating its effects.

7 | CONCLUSION

The current research has proposed a suitable model to deal with overvoltages induced by nearby LS in a PV array. This has extended our previous works [1, 8] by proposing a new modelling for the whole PV array that accounts for the proposed IMCMs and MGCM. The planned approach has the flexibility to represent different array groundings and configurations as well as external conditions such as the LC geometry and the LS spot distance. In addition, it is fast enough to allow MonteCarlo analyses. Thus, through simulations, the influence of these key factors on the lightning overvoltages in a case study of medium-size PV array is assessed. Moreover, in such a framework, the relevance of the IMCMs and MGCMs is assessed.

The comprehensive analysis of the coupling mechanisms conclusively reveals that MGCM strongly impacts only on variables related to frameground connections, that is, voltage and current, providing individually, the 102% and 91% of the reference case. The impact of the IMCM-CC becomes much smaller and can be omitted, while the impact of IMCM-IC moves the results away from the base case and towards the reference case.

The impact of the grounding configuration on voltages and currents induced in the array is usually quite small. However, at single module level, a drop in EM stress (about 35%) is attained in the ungrounded configuration for the differential-mode overvoltage; this is the most threatening effect to the PV insulation.

The overvoltages are closely related to the location of the lightning striking spot. Nonetheless, depending on the induced variable, related with PV array, module, or frame, this decreases less than, as, or more than the distance respectively. In addition, centred or off-centre location of the striking spot regarding the MS plays a primary role.

The impact of the grounding configuration proves the superiority of the HC configuration for the whole array and voltages frame to ground. However, it was observed that TCT is the

TABLE 8 Effect of the LC geometry (vertical strike corresponds to reference case at spot P5)

V_{out} (kV)		I_{out} (A)		V_{pv} (#1.2) (kV)		I_{pv} (#1.8) (A)		V_{gnd} (#4.1) (kV)		V_{fg} (#1.1) (V)		I_{fg} (#1.1) (A)	
Aver.	Stdev.	Vert. strike	Aver.	Stdev.	Vert. strike	Aver.	Stdev.	Vert. strike	Aver.	Stdev.	Vert. strike	Aver.	Stdev.	Vert. strike
−13.23	2.46	−15.1	−460.55	85.68	−523.11	−2.42	0.56	−2.59	−227.30	55.18	−253.65	−11.19	2.09	−12.73	−44.03	7.32	−54.09	−4.43	0.88	−4.99
Min.	Max.		Min.	Max.		Min.	Max.		Min.	Max.		Min.	Max.		Min.	Max.		Min.	Max.	
−6.94	−18.51		−241.72	−643.92		−1.29	−3.47		−95.26	−399.12		−5.84	−16.22		−29.18	−58.07		−2.29	−6.23	

most appropriate configuration for decreasing stress in single PV modules: a drop of up to 45% for common mode voltages and of 7% for voltages negative to ground can be observed in this case.

According to the tortuosity statistics, LC geometry leads to a non-negligible increase in the peak values in the variables, impacting both on currents and voltages, achieving up to 24% for most variables.

CONFLICT OF INTEREST

The authors do not have a conflict of interest.

FUNDING INFORMATION

No specific funding for this work was obtained.

DATA AVAILABILITY STATEMENT

Data available on request from the authors.

ORCID

Jesús De La Casa Hernández https://orcid.org/0000-0001-9117-1689

Alessandro Formisano https://orcid.org/0000-0002-7007-5759

REFERENCES

1. Formisano, A., Petrarca, C., Hernández, J.C., et al.: Assessment of induced voltages in common and differential-mode for a PV module due to nearby lightning strikes. IET Renewable Power Gener. 13, (8), 1369–1378 (2019)
2. Hernandez, J.C., Vidal, P.G., Jurado, F.: Lightning and surge protection in photovoltaic installations. IEEE Trans. Power Delivery 23(4), 1961–1971 (2008)
3. Zhang, Y., Chen, H., Du, Y.: Lightning protection design of solar photovoltaic systems. Electr. Power Syst. Res. 174, 105877 (2019)
4. Zhang, Y., Chen, H., Du, Y.: Considerations of photovoltaic system structure design for effective lightning protection. IEEE Trans. Electromagn. Compat. 62(4), 1–9 (2020)
5. Kalecz, G., Toth, Z., Kiss, I., et al.: Theory behind the zone concept for external lightning protection of photovoltaic power plants. Electr. Power Syst. Res. 209, 108025 (2022)
6. Kokkinos, N., Christofide, N., Charalambous, C.: Lightning protection practice for large-extended photovoltaic installations. In: Proceedings of International Conference on Lightning Protection. Vienna, pp. 1–5 (2012)
7. Stern, H., Karner, H.C.: Lightning induced EMC phenomena in photovoltaic modules. In: Proceedings of International Symposium on Electromagnetic Compatibility. Dallas, USA, pp. 442–446 (1993)
8. Formisano, A., Hernández, J.C., Petrarca, C., et al.: Modeling of PV module and DC/DC converter assembly for the analysis of induced transient response due to nearby lightning strike. Electronics 10, 1–12 (2021)
9. Naxakis, I., Christodoulou, C., Perraki, V., et al.: Degradation effects on single crystalline silicon photovoltaic modules subjected to high impulse-voltages. IET Sci. Meas. Technol. 11(5), 563–570 (2017)
10. NEDO. Analysis and evaluation of lightning damage condition and damage decrease countermeasure technique of lightning damage for PV systems. (2009)
11. CIGRE WG C4.408: Lightning protection of low-voltage networks. CIGRE Technical Brochure. (2013). https://e-cigre.org/publication/ELT_269_8-lightning-protection-of-low-voltage-networks-procedures
12. Formisano, A., Hernandez, J.C., Petrarca, C., et al.: Computation of coupling parameters between neighboring panels in photovoltaic arrays. In: Proceedings of International Conference on Computation Electromagnetic Fields. Cancun, Mexico, pp. 1–4 (2022)
13. Yang, H., Liu, X.: Design of PV charge and discharge controller in insulator monitoring system. In: Proceedings of International Conference on

Artificial Intelligence, Management Science and Electronic Commerce. Dengleng, pp. 2039–2042 (2011)
14. Sekioka, S.: An experimental study of sparkover between a rod and a photovoltaic panel. In: Proceedings of International Conference on Lightning Protection. Vienna, Austria, pp. 1–5 (2012)
15. Mendez, Y., Acosta, I., Rodriguez, J.C., et al.: Effects of the PV-generator's terminals connection to ground on electromagnetic transients caused by lightning in utility scale PV-plants. In: Proceedings of International Conference on Lightning Protection. Estoril, pp. 1–8 (2016)
16. Tu, Y., Zhang, C., Hu, J., et al.: Research on lightning overvoltages of PV arrays in a rooftop photovoltaic power system. Electr. Power Syst. Res. 94, 10–15 (2013)
17. Benesova, Z., Haller, R., Birkl, J., et al.: Overvoltages in photovoltaic systems induced by lightning strikes. In: International Conference on Lightning Protection. Vienna, pp. 1–6 (2012)
18. Fuangfung, Y., Sinthusonthishat, S., Yutthagowith, P.: A software tool for induced voltages and currents calculation caused by lightning electromagnetic field in PV systems. In: Proceedings of International Conference on Electrical Engineering/Electronics, Computer, Telecommunications and Information Technology. Hua Hin, pp. 1–4 (2015)
19. Takada, T., Ishii, M.: Lightning-induced voltages around PV panel on ground. In: Proceedings of IEEJ Technical Meeting on HV Engineering. HV-11-90, 2011–12
20. Azhari, M.E.: Lightning-induced voltage on DC power line of PV panel. Masters dissertation. The University of Tokyo (2013)
21. Fallah, N., Gomes, C., Kadir, M.Z.A.A.: Lightning protection techniques for roof-top PV systems. In: Proceedings of International Conference on Power Engineering and Optimization. Langkawi, Malaysia, pp. 1–4 (2013)
22. Sakai, K., Yamamoto, K.: Lightning protection of photovoltaic power generation system: Influence of grounding systems on overvoltages appearing on DC wirings. In: Proceedings of International Symposium on Lightning Protection. Belo Horizonte, pp. 335–339 (2013)
23. Yamamoto, K., Takami, J., Okabe, N., et al.: Overvoltages on DC side of power conditioning system caused by lightning stroke to structure anchoring PV panels. Electr. Eng. Jpn. 187(4), 29–41 (2014)
24. Karim, M.R., Ahmed, M.R.: Lightning effect on a large-scale solar power plant with protection system. In: Proceedings of International Conference on Advances in Science, Engineering and Robotics Technology (ICASERT). Dhaka, Bangladesh, pp. 1–5 (2019)
25. Zaini, N., Ab-Kadir, M., Izadi, M., et al.: On the effect of lightning on a solar photovoltaic system. In Proceedings of the International Conference on Lightning Protection (ICLP). Estoril, Portugal, 1–4 (2016)
26. Zaini, N.H., Kadir, M.Z.A.A., Radzi, M.A.M., et al.: Lightning surge analysis on a large-scale grid-connected solar photovoltaic system. Energies 10, 2149 (2017)
27. Sabiha, N.A., Alsharef, M., Metwaly, M.K., et al.: Sustaining electrification service from photovoltaic power plants during backflow lightning overvoltages. Electr. Power Syst. Res. 186, 106386 (2020)
28. Snodgrass, J., Xie, L., et al.: Overvoltage analysis and protection of lightning arresters in distribution systems with distributed generation. Int. J. Electr. Power Energy Syst. 123, 106209 (2020)
29. Jiang, T., Grzybowski, S.: Electrical degradation of Photovoltaic modules caused by lightning induced voltage. In: Proceedings of IEEE International Conference on Electrical Insulation. Philadelphia, PA, pp. 107–110 (2014)
30. Demirel, E., Dolgun, G.K., Keçebaş, A.: Comprehensive transient analysis on control system in a photovoltaic power plant under lightning strike. Sol. Energy 233, 142–152 (2022)
31. Sun, Q., Zhong, X., Zhong, L., et al.: Investigation on induced voltage of photovoltaic system on complex terrain. Electr. Power Syst. Res. 201, 107549 (2021)
32. Sun, Q., Zhong, X., Liu, J., et al.: Three-dimensional modeling on lightning induced overvoltage for photovoltaic arrays installed on mountain. J. Cleaner Prod. 288, 125084 (2021)
33. Zhang, Y., Chen, H., Du, Y., et al.: Transients in solar photovoltaic systems during lightning strikes to a transmission line. Int. J. Electr. Power Energy Syst. 124, 106885 (2022)
34. Zhang, Y., Li, B., Du, Y., et al.: Effective grounding of the PV power plant protected by lightning rods. IEEE Trans. Electromagn. Compat. 63, 1128–36 (2021)
35. Sabiha, N.A., Alsharefa, M., Metwalya, M.K., et al.: 'Sustaining electrification service from photovoltaic power plants during backflow lightning overvoltages. Electr. Power Syst. Res. 186, 106386 (2020)
36. Hetita, I., Zalhaf, A.S., Mansour, D.A., et al.: Modeling and protection of PV systems during lightning strikes: A review. Renewable Energy 184, 134–148 (2022)
37. Dechthummarong, C., Chenvidhya, D., Jivacate, C., et al.: Experiment and simulation impulse partial discharge behavior in dielectric encapsulations of field-aged PV modules. In: Proceedings of IEEE Photovoltaic Specialists Conference. Seattle, pp. 3109–3112 (2011)
38. Charalambous, C.A., Kokkinos, N.D., Christofides, N.: External lightning protection and grounding in large-scale photovoltaic applications. IEEE Trans. Electromagn. Compat. 56(2), 427–434 (2014)
39. Hernández, J.C., Vidal, P.G., Medina, A.: Characterization of the insulation and leakage currents of PV generators: Relevance for human safety. Renewable Energy 35(3), 593–601 (2010)
40. Di Piazza, M.C., Viola, F., Vitale, G.: Evaluation of ground currents in a PV system with high frequency modeling. Int. J. Renewable Energy Res. 8(3), 1170–1178 (2018)
41. Coetzer, K.M., Wiid, P.G., Rix, A.J.: PV installation design influencing the risk of induced currents from nearby lightning strikes. In: Proceedings of International Conference on Clean Electrical Power (ICCEP). Otranto, Italy, pp. 204–213 (2019)
42. Haeberlin, H.: Interference voltages induced by magnetic fields of simulated lightning currents in photovoltaic modules and arrays. In: Proceedings of European Conference on Photovoltaic Solar Energy. Munich, Germany, pp. 1–4 (2001)
43. Hernandez, J.C., Vidal, P.G., Medina, A.: Characterization of the insulation and leakage currents of PV generators: Relevance for human safety. Renewable Energy 35, 593–601 (2010)
44. Yu, S., Wang, J., Zhang, X.: Complete parasitic capacitance model of photovoltaic panel considering the rain water. Chin. J. Electr. Eng. 3(3), 77–84 (2017)
45. Hossain, A., Ahmed, R.: Analysis of indirect lightning phenomena on solar power system. J. Electr. Eng. 21(4), 127–133 (2014)
46. Balato, M., Costanzo, L., Vitelli, M.: Series-parallel PV array reconfiguration: Maximization of the extraction of energy and much more. Appl. Energy 59, 145–160 (2015)
47. Belhachat, F., Larbes, C.: Modeling, analysis and comparison of solar photovoltaic array configurations under partial shading conditions. Sol. Energy (120), 399–418 (2015)
48. Ramaprabha, R., Mathur, B.L.: A comprehensive review and analysis of solar photovoltaic array configurations under partial shaded conditions. Int. J. Photoenergy 2012, 120214 (2012)
49. Patel, H., Agarwal, V.: MATLAB-based modeling to study the effects of partial shading on PV array characteristics. IEEE Trans. Energy Convers. 23, 302–310 (2008)
50. Díaz-Dorado, E., Cidrás, J., Carrillo, C.: Discrete I–V model for partially shaded PV-arrays. Sol. Energy 103, 96–107 (2014)
51. Bingol, O., Ozkaya, B.: Analysis and comparison of different PV array configurations under partial shading conditions. Sol. Energy 160, 336–343 (2018)
52. Malathy, S., Ramaprabha, R.: Comprehensive analysis on the role of array size and configuration on energy yield of photovoltaic systems under shaded conditions. Renewable Sustainable Energy Rev. 49, 672–679 (2015)
53. Ramos-Paja, C.A., Bastidas, J.D.: Experimental validation of a model for photovoltaic arrays in total-cross-tied configuration. Dyna 80, 191–199 (2013)
54. Kaushika, N.D., Gautam, N.K.: Energy yield simulations of interconnected solar PV arrays. IEEE Trans. Energy Convers. 18, 127–134 (2003)
55. Bastidas-Rodriguez, J., Ramos-Paja, C., Trejos-Grisales, A.: Mathematical model of bridge-linked photovoltaic arrays operating under irregular. Tecno Lógicas., ISSN 0123-7799, Edición Especial, 223–235 (2013)

56. Ogata, K.: Modern Control Engineering. Prentice Hall, New York (1976)
57. IEC standard: EN 62305-2: Protection against lightning—part 2: Risk management. (2020)
58. Thomson, J.J.: Recent Researches in Electricity and Electromagnetism. pp. 208–250. Clarendon Press, Oxford (1983)
59. Paul C.R.: Introduction to Electromagnetic Compatibility. Wiley & Sons, New York (2005)
60. Bueno-Barrachina, J.M., Cañas-Peñuelas, C.S., Catalan-Izquierdo, S.: Capacitance evaluation on non-parallel thick-plate capacitors by means of finite element analysis. J. Energy Power Eng. (5), 373–378 (2011)
61. Bastidas-Rodríguez, J.D., Trejos-Grisales, L.A., González-Montoya, D., Ramos-Paja, C.A., Petronee, G., Spagnuolo, G.: General modeling procedure for photovoltaic arrays. Electr. Power Syst. Res. 155, 67–79 (2018)
62. Wang, Y.-J., Hsu, P.-C.: An investigation on partial shading of PV modules with different connection configurations of PV cells. Energy 36, 3069–3078 (2011)
63. Yadav, A.S., Pachauri, R.K., Chauhan, Y.K.: Comprehensive investigation of PV arrays with puzzle shade dispersion for improved performance. Sol. Energy 129, 256–285 (2016)
64. Ghosh, S., Yadav, V.K., Mukherjee, V.: Evaluation of cumulative impact of partial shading and aerosols on different PV array topologies through combined Shannon's entropy and DEA. Energy 144, 765–775 (2018)
65. IEC standard. 60664-1: Insulation coordination for equipment within LV systems—part 1: Principles, requirements and tests. (2020)
66. IEC standard. 61000-4-5: Electromagnetic compatibility—part 4–5: Testing and measurement techniques—surge immunity test. (2017)
67. IEC standard. 61730–2: PV module safety qualification—part 2: Requirements for testing. (2016)

How to cite this article: Hernández, J.C., Sanchez-Sutil, F., Petrarca, C., Formisano, A.: A study on the effects of electromagnetic coupling mechanisms in the event of an indirect lightning strike near photovoltaic arrays. IET Renew. Power Gener. 1–16 (2022). https://doi.org/10.1049/rpg2.12646